Research on the granular flow based on discrete element method

Minglong You(1), Liping Liu(2), Jingze Shi(3),
China University of Geosciences
Wuhan, China
Minglong You ： 1906809001@qq.com
Liping Liu：liuliullp@163.com
Jingze Shi：446972000@qq.com

***Abstract*—The destabilizing and destructive motion of a granular column pile is a complex process containing sliding, translation, and rotation with macroscopic discontinuities and randomness of individual block motion. In order to study the geometric characteristics of the sand after the rapid release of sand granular columns, this study simulates the motion of sand piles with different aspect ratios (H/L) under the rapid withdrawal of baffles with the aid of the particle discrete element software PFC. By simulating the particle accumulation morphology of sand piles with different aspect ratios (H/L) at a single baffle, the fine-scale parameters of particles were calibrated and the simulation results were in high agreement with the experimental results. Finally, two sets of cubic sand piles with different aspect ratios were simulated, and the pile height, transport distance and pile bottom angle of sand particles after settling were predicted. The results show that the particle discrete element software PFC can well simulate the motion of sand columnar piles after fast extraction of the baffle with high accuracy and reliability.**

Keywords*—Granular column; Sand pile morphology; Accumulation range; Discrete element method; Numerical simulation

I. Principle of the discrete element method and particle discrete element PFC software

In order to solve the discontinuous mechanical problems such as crack

propagation in geotechnical engineering, Cundall proposed the discrete element method based on the discontinuous medium mechanics method in the last century, which was initially used to analyze the slip damage process of rocky slopes containing joint fissures. Compared with the traditional method of continuous medium mechanics, its advantage is that it can simulate the contact force and displacement of the contact surface between the rock masses, and can obtain the stress-strain data inside the rock masses in time[1].

Cundall proposed the particle discrete element method based on the block discrete element in order to better analyze the mechanics of the bulk media, and developed a commercial numerical calculation software (PFC2D/PFC3D) based on this calculation method[2]. The fracture damage problem is better presented from a fine viewpoint and has its unique advantages in the numerical simulation study of the process of fracture initiation and propagation in rock masses. In previous studies of rocks it has been found that the microscopic properties of rocks, such as the composition, arrangement, particle bonding, particle gradation and size of rock mineral particles, can have an impact on the macroscopic mechanical parameters and mechanical behavior of rocks[3], so it is different from the general numerical simulation. The particle discrete element needs to set the mesoscale parameters of the particle and contact models, which correspond to the macroscopic mechanical parameters of the rock mass but are slightly different, and need to combine the basic theories of fracture mechanics and contact mechanics to reach the equivalent substitution between macroscopic and mesoscale. Particle discrete elements are not only widely used in the field of geotechnical engineering, but also play an increasingly important role in many industrial fields such as unconventional oil and gas extraction, stability evaluation of surrounding rock in deep buried tunnel, road materials, and mining.

1.1 Basic assumptions

The particle discrete element method has the following assumptions in the numerical calculation.

(1) The particle spheres are all rigid bodies and will not be deformed by any

collisional forces.

(2) The particle-to-particle contact model and parameters can be freely set according to the actual situation.

(3) Although the particles are rigid bodies, a small overlap is allowed between the particles.

(4) In PFC software, a rigid cluster (Clump) function can be employed to assemble multiple rigid spherical particles into arbitrary shape rigid blocks, and the blocks are not separable from each other; through the flexible cluster (Cluster) function, multiple rigid spherical particles can be assembled into arbitrary shape flexible blokcs through the contact model, and these blocks can be separated into spherical particles again under the action of force.

As shown in Fig. 1, the calculation method used by the PFC software is an explicit iterative method, which iterates cyclically based on the Newton's second law of motion and the force-displacement law.

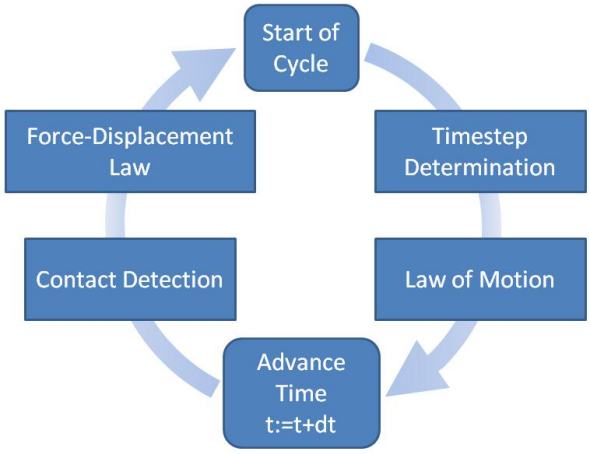

Fig. 1 Explicit cycle calculation process of PFC software

1.2 Model components

Each particle in a PFC model is denoted as a body to clarify the fact that it is not a point mass; a body is a discrete, rigid body with finite extent and a well-defined surface, as shown in Fig. 2. The PFC model consists of bodies, pieces, and contacts. There are three types of bodies: balls, clumps, and walls. Each body is composed of one or more pieces. A ball is a unit-thickness disk in 2D or sphere in 3D. A clump is a collection of pebbles that are unit-thickness disks in 2D or spheres in 3D. Clumps

model can be arbitrary shape rigid bodies. The pebbles that make up a clump can overlap, but contacts do not exist between them; instead, there are contacts between the pebbles and the pieces of other bodies. A wall is a collection of facets that are linear segments in 2D or triangles in 3D, and that form a manifold and orientable surface. Bodies may have surface properties that can be assigned to each piece on the body surface; these surface properties may be used to determine the piece interactions. Bodies exist within the model domain and cannot move outside of this region.

The motion of balls and clumps obeys Newton's laws of motion, but the motion of walls is user-specified; thus, only balls and clumps have mass properties (mass, centroid position, and inertia tensor) and loading conditions (the force/moment applied from contacts, a body force arising from gravity, and an externally applied force/moment).

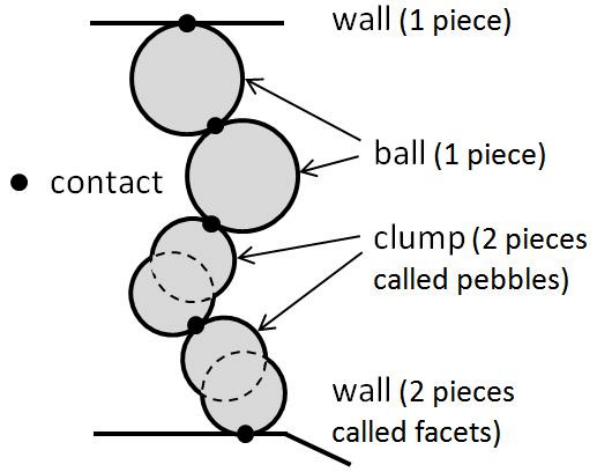

Fig. 2 Schematic diagram of blocks in PFC model

1.3 The force-displacement law

In the particle-discrete element method, the contact model will use the force-displacement law, and the contact is divided into two types of contact, i.e., particle-particle contact and particle-wall contact. The particle-particle contact is shown in Fig. 3, and the direction of the line between the centers of the two particles is considered as the normal direction of the contact. As shown in Fig. 4 for particle-wall contact, the direction of the line from the center of the particle to the wall is considered as the normal direction of this contact. The distance between the particle and the particle form center can be calculated according to the following

equation.

$$d=\left|x_i^{[B]}-x_i^{[A]}\right|=\sqrt{\left(x_i^{[B]}-x_i^{[A]}\right)\left(x_i^{[B]}-x_i^{[A]}\right)} \tag{1}$$

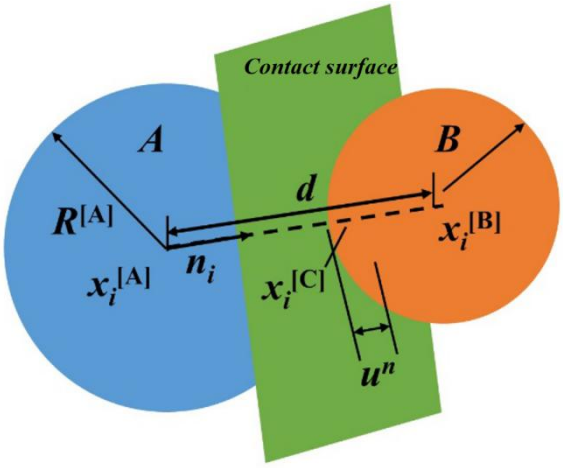

Fig. 3 Schematic diagram of particle contact

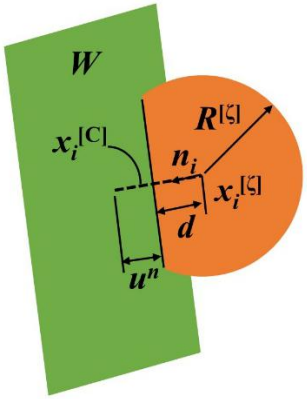

Fig. 4 Schematic diagram of particle contact with the wall

The PFC allows a small overlap of objects in contact, and the amount of overlap U^n can be calculated according to the following equation:

$$U^n=\begin{cases} R^{[A]}+R^{[B]}-d & particle\ contact \\ R^{[b]}-d & particle\ contact\ with\ the\ wall \end{cases} \tag{2}$$

where R is the value of the radius length of the particle; the value of the position vector of the contact point can be calculated by the following equation.

$$x_i^{[C]}=\begin{cases} x_i^{[A]}+(R^{[A]}-\dfrac{1}{2}U^n)n_i \\ x_i^{[b]}+(R^{[b]}-\dfrac{1}{2}U^n)n_i \end{cases} \tag{3}$$

The contact force F_i can be decomposed by the orthogonal decomposition method

into the components along the normal direction F_i^n and the tangential direction F_i^s:

$$F_i = F_i^n + F_i^s \tag{4}$$

The normal component F_i^n can be calculated from the following equation:

$$F_i^n = K^n U^n n_i \tag{5}$$

where K^n is the normal directional stiffness of the contact. The tangential relative velocity at the point of contact between the two particles V^S can be expressed by the calculation of Eq. (6):

$$V^S = (\dot{x}_i^{[\phi^2]} - \dot{x}_i^{[\phi^1]})\mathbf{t}_i - \omega^{[\phi^2]}\left|x_k^{[C]} - x_k^{[\phi^2]}\right| - \omega^{[\phi^1]}\left|x_k^{[C]} - x_k^{[\phi^1]}\right| \tag{6}$$

where: $\dot{x}_i^{[\phi^2]}$ denotes the translational velocity of the particle, $\omega^{[\phi^2]}$ denotes the rotational velocity of the particle, the tangential direction vector $\mathbf{t}_i = (-n_2, n_1)$. The increment of displacement component in the tangential direction of the spherical particle ΔU_i^s in one time step Δt can be expressed as

$$\Delta U_i^s = V_i^s \Delta t \tag{7}$$

The resulting contact force component in the tangential direction of the spherical particles , ΔF_i^s, can be expressed as

$$\Delta F_i^s = -K^s \Delta U_i^s \tag{8}$$

where K_s denotes the tangential stiffness at the contact point of the two particles; V_i^s denotes the tangential velocity component at the contact point. By continuously accumulating the tangential directional contact force components of the spherical particles calculated in the previous time step, the tangential directional contact force components of the current time step can be calculated by the following equation.

$$F^s \leftarrow F^s + \Delta F^s \le \mu F^n \tag{9}$$

where μ indicates the coefficient of friction of the ball particles. The combined force and combined moment acting between two contacting objects can be expressed by the following equation

$$
\begin{aligned}
&F_i = F^n n_i + F^s t_i \\
&F_i^{[\Phi^1]} \leftarrow F_i^{[\Phi^1]} - F_i \\
&F_i^{[\Phi^2]} \leftarrow F_i^{[\Phi^2]} + F_i \\
&M_3^{[\Phi^1]} \leftarrow M_3^{[\Phi^1]} - e_{3jk}(x_j^{[C]} - x_j^{[\Phi^1]})F_k \\
&M_3^{[\Phi^2]} \leftarrow M_3^{[\Phi^2]} + e_{3jk}(x_j^{[C]} - x_j^{[\Phi^2]})F_k
\end{aligned}
\tag{10}
$$

1.4 Equations of motion

In the calculation of the discrete element of the particle, since the particle is a rigid body, there are only two kinds of motion of the particle: parallel motion and rotation around the center. The physical quantities used in the parallel motion of the particle are: particle coordinates x_i , velocity $\dot{x}_i$ and acceleration $\ddot{x}_i$, and the following physical quantities are used in the rotation of the particle around the center: angular velocity of rotation ω_i and angular acceleration of rotation $\dot{\omega}_i$. Because the physical quantities of motion are vectors, the motion of the particle can be expressed by the following two vector equations.

Equation of parallel motion in vector form:

$$F_i = m(a - g_i) \tag{11}$$

where F_i is the vector sum of the external forces acting on the spherical particle; m is the mass; g denotes the acceleration of gravity.

The vector equation of rotation around the center is shown as follow:

$$M_i = \dot{H}_i \tag{12}$$

where M_i is the vector sum of all external moments acting on the spherical particle; $\dot{H}_i$ denotes the angular momentum of the spherical particle. The Euler equation of motion can be obtained from Eq. (12) as follows:

$$
\begin{aligned}
M_1 &= I_1\dot{\omega}_1 + (I_3 - I_2)\omega_3\omega_2 \\
M_2 &= I_2\dot{\omega}_2 + (I_1 - I_3)\omega_1\omega_3 \\
M_3 &= I_3\dot{\omega}_3 + (I_2 - I_1)\omega_2\omega_1
\end{aligned}
\tag{13}
$$

where $\dot{\omega}_1, \dot{\omega}_2, \dot{\omega}_3$ denote the angular acceleration in three different directions of the spherical particle, respectively; M_1, M_2, M_3 are the components of the combined

moment applied to the spherical particle along each coordinate axis, respectively; I_1, I_2, I_3 are the components of the moment of inertia of the particle along the direction of the spatial coordinate axis, which are of equal value in the spherical particle. For the disc-shaped particles, since the value of the moment of inertia in its out-of-plane direction is zero, equation (1.13) can be expressed as

$$M_3 = I_3\dot{\omega}_3 = (\beta m R^2)\dot{\omega} \qquad where \beta = 1/2 \tag{14}$$

II. Numerical modelling

Using PFC software, the computational domain was established, and the wall was built as a model box for particle column stacking according to the model size in the test. The geometry of the model box was 1500mm*400mm*1000mm, the spacing between the single baffle and the left boundary of the container was 200mm in the calibration test, the spacing between the single baffle and the left boundary of the container was also 200mm in the prediction test, and the spacing between the two baffles was 200mm and 310mm in turn. After the establishment of the wall model, the establishment of the spherical particle model was completed according to the different aspect ratio of the particle column in turn, and the wall model is shown in Fig. 5.

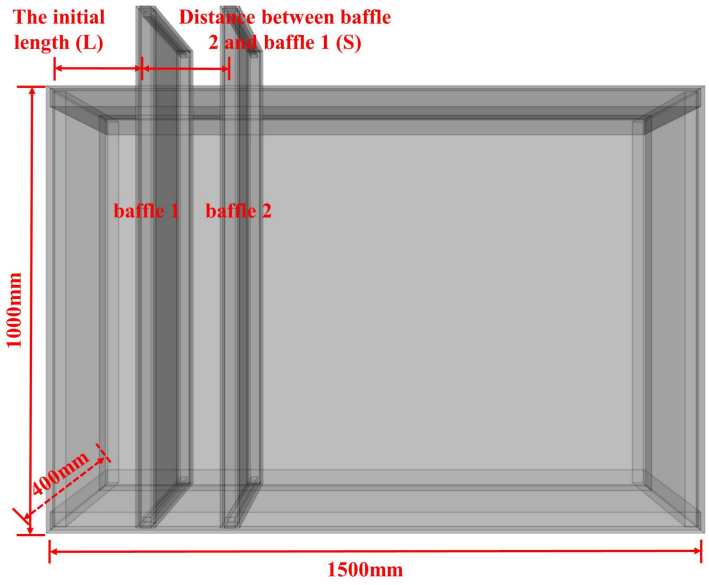

Fig. 5 Schematic of the model box

The simulation is divided into two parts: the first part is a calibration test, in which a baffle is set on the right side of the sand pile particles, then the baffle is

quickly extracted; the second part is a prediction test, in which two baffles are set on the right side of the sand pile particles, and the distance between the two baffles is S. The pile height of the standard sand pile transported to the second baffle is predicted. The mesoscale parameters of model are listed in Table 1.

Table 1 Mesoscale parameters of discrete elements of particles

Parameters	value
Minimum particle size R_{min} (m)	0.004
R_{max}/R_{min}	1.25
Effective modulus (Pa)	1.0e6
Kratio	1.0
Fric	0.35
Density (kg/m^3)	1600

There are four groups of calibration simulations, and the specific parameters of the simulated sand pile are shown in Table 2.

Table 2 Single baffle parameters table

No.	Number of particles	Initial length L (mm)	Initial height H (mm)	Aspect Ratio (H/L)
1	26961	200	200	1
2	53891	200	400	2
3	80800	200	600	3
4	53968	400	200	0.5

The model of calibration group is shown in Fig. 6.

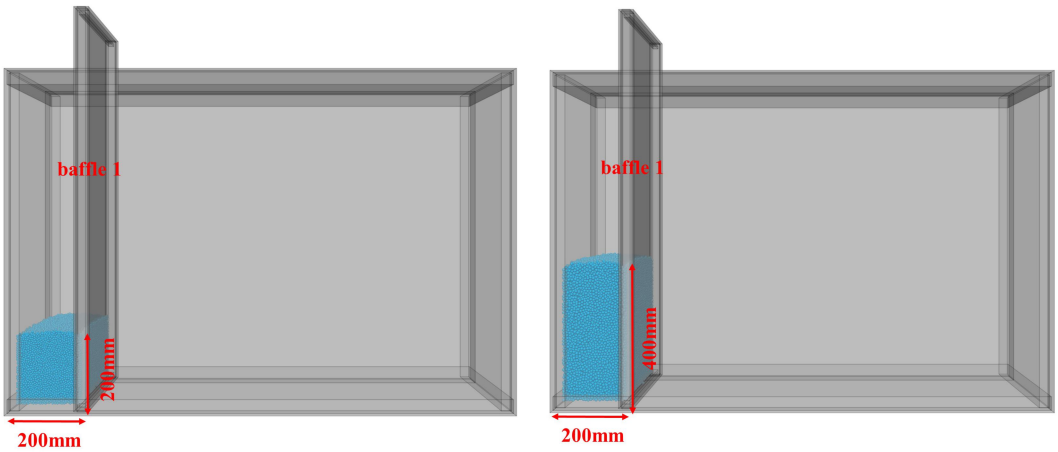

(a)H/L=1 (b) H/L=2

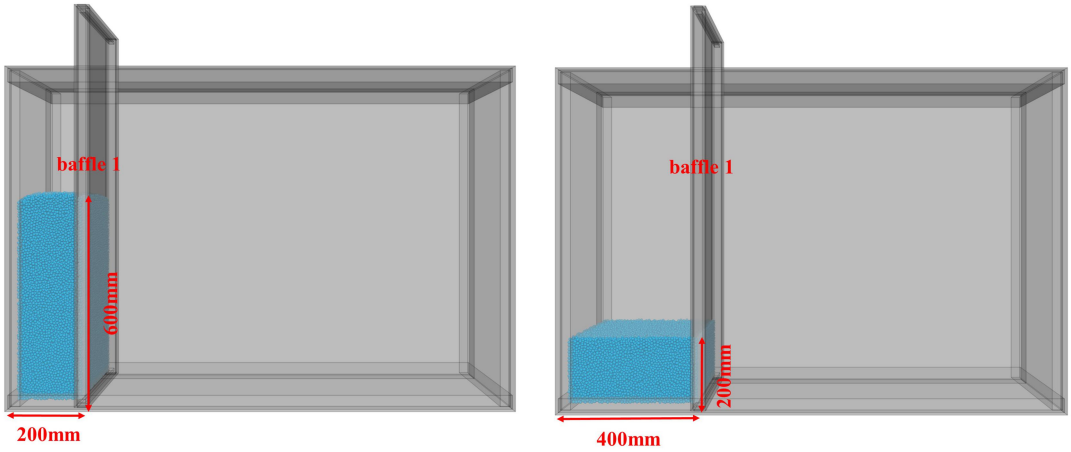

(c) H/L=3 (d) H/L=0.5

Fig. 6 Calibration group model

Two sets of prediction simulations were performed, and the specific parameters of the simulated sand piles are shown in Table 3.

Table 3 Parameters in double baffles test

NO.	Number of particles	Initial length L (mm)	Initial height H (mm)	Distance between baffle 2 and1 S (mm)	Aspect Ratio (H/L)
5	50533	200	400	200	2
6	79384	200	600	310	3

The prediction group models are shown in Fig. 7.

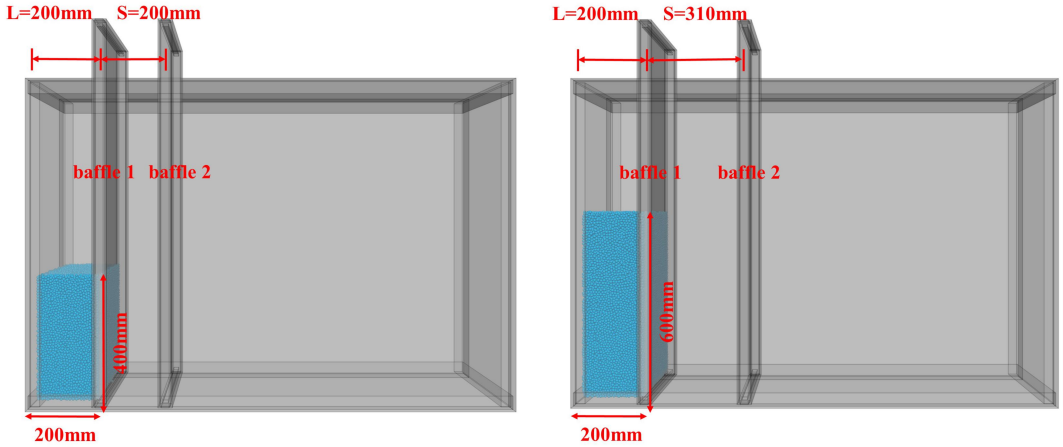

(a)H/L=2 (b)H/L=3

Fig. 7 Prediction group models

III. Calibration results

The results (displacement) of the calibration group are shown in Fig. 8.

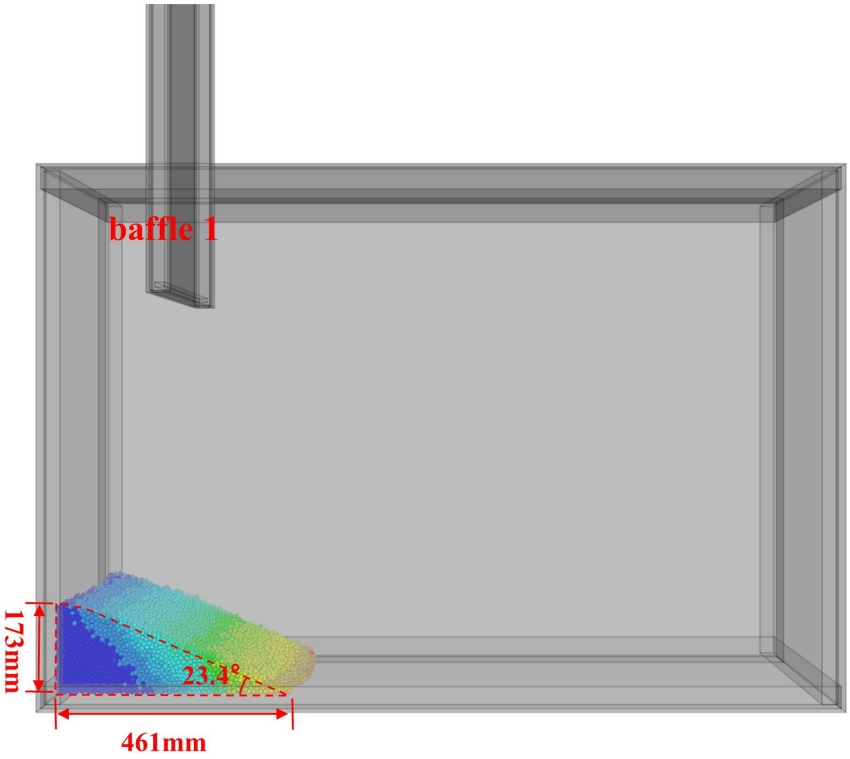

(a) H/L=1

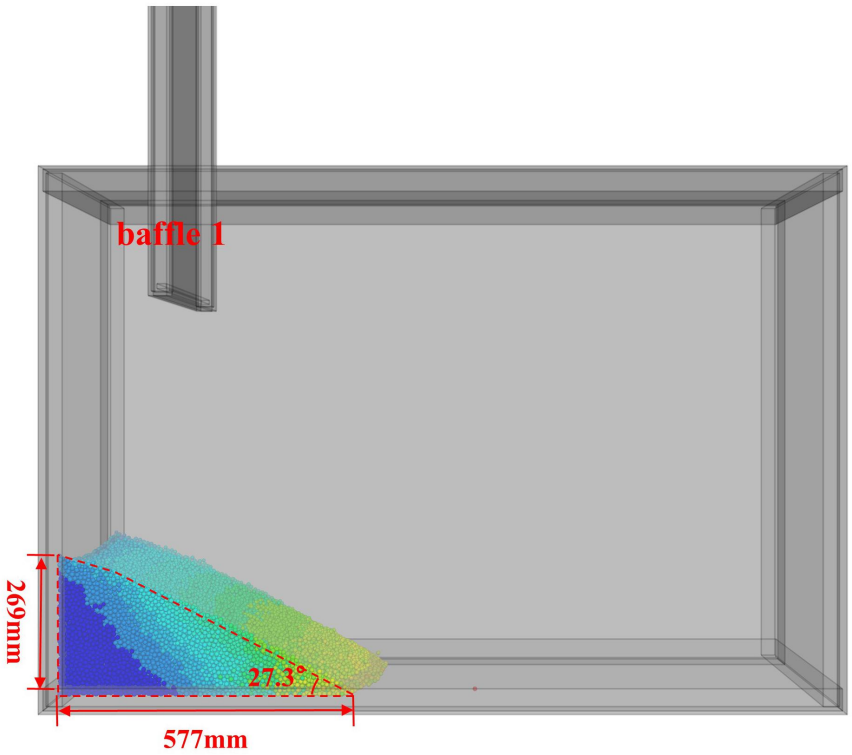

(b) H/L=2

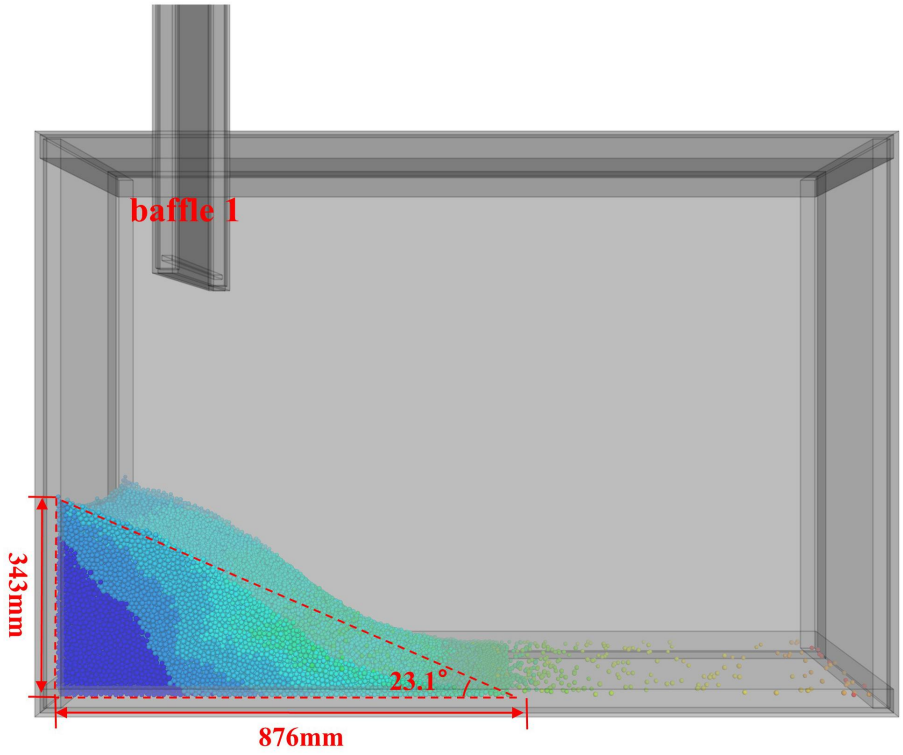

(c) H/L=3

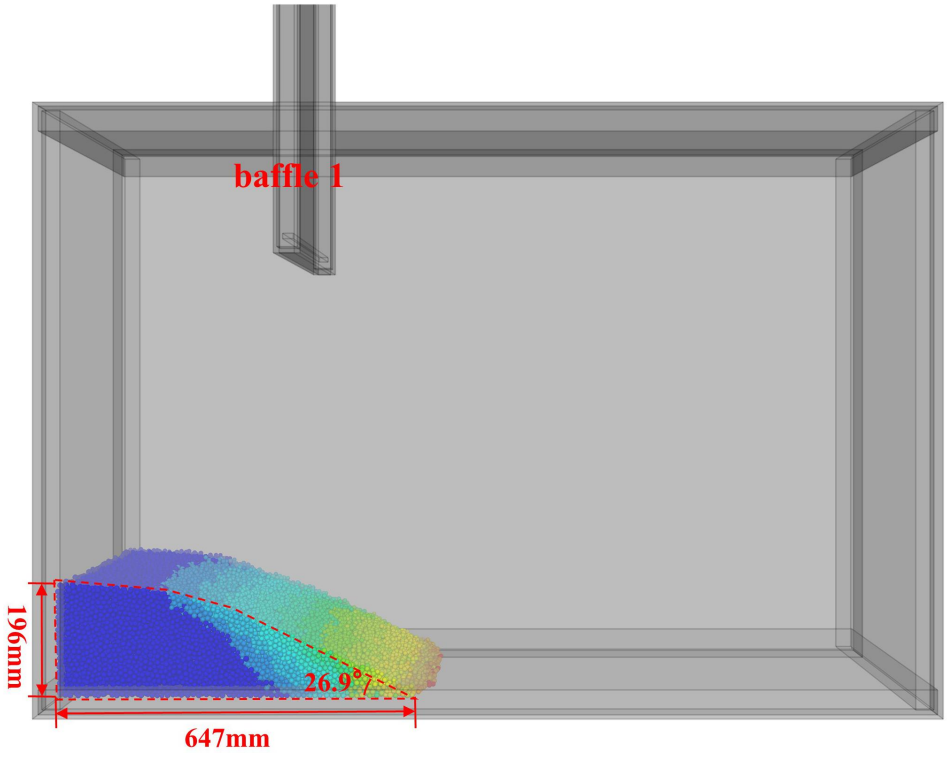

(d) H/L=0.5

Fig. 8 Results of calibration group

The calibration results are shown in Table 4.

Table 4 Results of calibration tests

No.	Height after deposition H (mm)		Length after deposition L (mm)		Inclination (°)	
	Simulation	Test	Simulation	Test	Simulation	Test
1	173	200	461	420	23.4	29.5
2	269	310	577	620	27.3	26.5
3	343	380	876	920	23.1	22.0
4	196	200	647	650	26.9	27.0

It can be seen that the sand pile morphology is basically consistent with that in the test. The stacking range of the sand pile, i.e., the height of the pile, the transport distance of the pile and the bottom angle of the pile can be measured by using the tools in PFC, and the four sets of calibration results are basically consistent with the test. The height of the granular column up to 200 mm in the test remained constant after stacking. In PFC, the particle sliding friction coefficient has a significant effect on the stacking height and stacking angle, and the larger the friction coefficient, the larger the stacking height and the smaller the stacking length . If a larger friction coefficient is used to ensure that the simulated stacking height is absolutely consistent with that in the test, a reasonable stacking length cannot be obtained. To ensure the joint accuracy of height and length, a suitable friction coefficient is chosen so that both the stacking height and length are relatively close.

IV. Prediction results

According to the comparison of the simulation results of the first four groups of calibration tests, the correctness of the PFC model is verified, so the prediction of the sand pile accumulation height and pile bottom angle under the double baffle condition can be made, and the prediction model diagram has been given in Section III, and the calculation model of each prediction group is shown in Fig. 9.

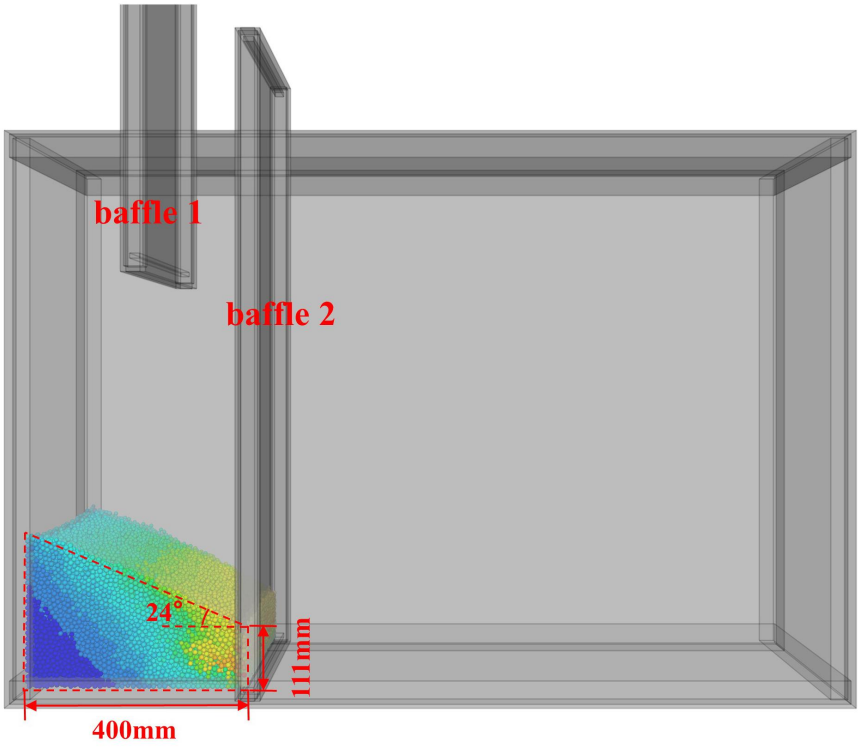

(a) H/L=2 (S=200mm)

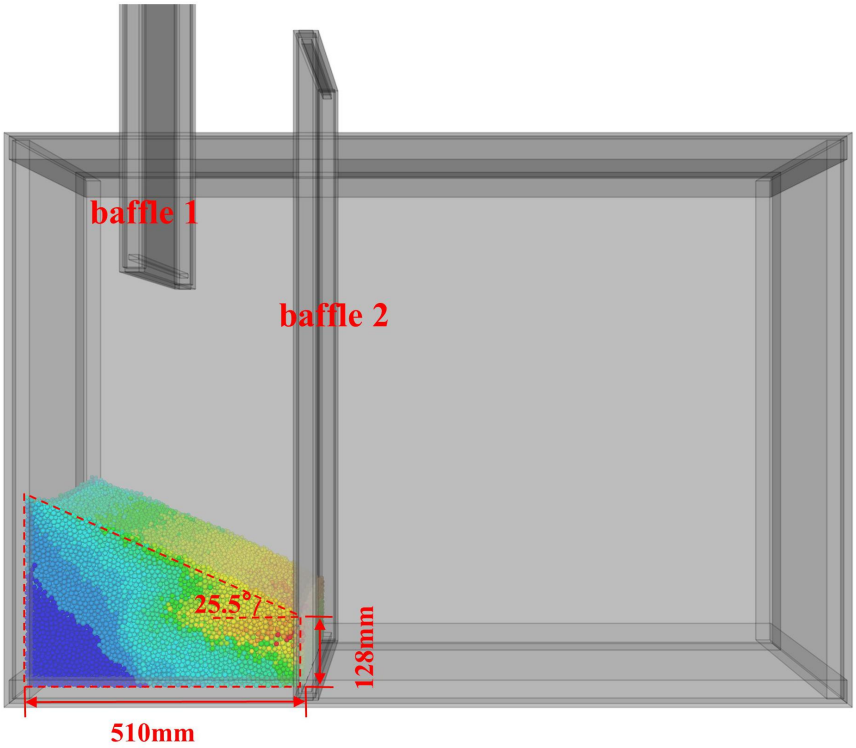

(b) H/L=3 (S=310mm)

Fig. 9 The calculation results of the prediction group

PFC was used to measure the stacking height and bottom stacking angle of the

sand pile at the second baffle, and the predicted results are shown in Table 5.

Table 5 Parameters of prediction results

No.	Height of sand at baffle 2 *H* (mm)	Inclinations (°)
5	111	24
6	128	25.5

V. Conclusions

In this study, the motion of sand piles with different aspect ratios (*H*/*L*) after fast extraction baffles was simulated with the aid of particle discrete element software PFC. The following results were obtained in the study.

(1) The results of the particle stacking column with a single baffle based on the particle discrete element software PFC simulation are in good agreement with the experimental results, and the modeling method and the mesoscale parameters of particle are reliable.

(2) On the basis of the parameter calibration, the results obtained of the particle stacking column with double baffle have high reliability, and according to the measurement results, we get: the height after deposition of the particle column with the size of 200mm*400mm*400mm is 111mm, and the bottom angle of the stack is 24°; the height after deposition of the particle column with the size of 200mm*400mm*600mm is 128mm, and the bottom angle of the pile is 25.5°.

References

[1] Cundall P A. A computer model for simulating progressive large scale movements in blocky rock systems[C]. Proceedings of Symposium Rock Fracture (ISRM), Nancy, France, 1971, Paper II-8.

[2] Cundall P A, Strack O D L. A discrete numerical model for granular assemblies[J]. Geotechnique, 1979, 29(1): 47-65.

[3] Li X, Feng Z, Han G, et al. Breakdown pressure and fracture surface morphology of hydraulic fracturing in shale with H2O, CO2 and N2[J]. Geomechanics and Geophysics for Geo-Energy and Geo-Resources, 2016, 2(2): 63-76.